

## **Algorithm Theoretical Basis Document**

### **Microwave Imager Radiance FCDR**

### **SMMR Brightness Temperatures**

**DOI: 10.5676/EUM\_SAF\_CM/FCDR\_MWI/V004**

**Microwave Imager Radiance FCDR R4**

**CM-12003**

Reference Number:


**SAF/CM/DWD/ATBD/FCDR\_SMMR**

Issue/Revision Index:

**2.3**

Date:

**2022-03-31**

	<b>Algorithm Theoretical Basis Document</b> <b>Microwave Imager Radiance FCDR R4</b> <b>SMMR Brightness Temperatures</b>	Doc. No: SAF/CM/DWD/ATBD/FCDR_SMMR Issue: 2.3 Date: 2022-03-31
---	--	--

## Document Signature Table

	Name	Function	Signature	Date
Author	Karsten Fennig	CM SAF Scientist		2022-03-31
Editor	Marc Schröder	Science Coordinator		2022-03-31
Approval	CM SAF Steering Group			
Release	Rainer Hollmann	Project Manager		


## Distribution List

Internal Distribution	
Name	No. Copies
DWD / Archive	1
CM SAF Team	1

External Distribution		
Company	Name	No. Copies
PUBLIC		1

## Document Change Record

Issue/ Revision	Date	DCN No.	Changed Pages/Paragraphs
1.0 draft	2015-11-10	SAF/CM/DWD/ATBD/FCDR_SMMR	Draft version for review.
1.1	2015-12-01	SAF/CM/DWD/ATBD/FCDR_SMMR	Final version after PCR.
2.0	2018-12-10	SAF/CM/DWD/ATBD/FCDR_SMMR	Version for PCR 3.1.
2.1	2019-02-05	SAF/CM/DWD/ATBD/FCDR_SMMR	Final version after PCR.
2.2	2022-01-31	SAF/CM/DWD/ATBD/FCDR_SMMR	Version for DRR 3.1
2.3	2022-03-31	SAF/CM/DWD/ATBD/FCDR_SMMR	Final version after DRR 3.1

	<b>Algorithm Theoretical Basis Document</b> <b>Microwave Imager Radiance FCDR R4</b> <b>SMMR Brightness Temperatures</b>	Doc. No: SAF/CM/DWD/ATBD/FCDR_SMMR Issue: 2.3 Date: 2022-03-31
---	--	--

## Applicable documents

Reference	Title	Code / Validity Date
AD 1	Memorandum of Understanding between CM SAF and the Max-Planck Institute for Meteorology and Meteorological Institute, University of Hamburg	1. March 2012
AD 2	Agreement between the European Organisation for the Exploitation of Meteorological Satellites (EUMETSAT) and the Federal Republic of Germany represented by the Deutsche Wetterdienst on the Continuous Development and Operations Phase of a EUMETSAT Satellite Application Facility in Climate Monitoring	1. December 2006
AD 3	CM SAF Product Requirements Document	SAF/CM/DWD/PRD/3.2

## Reference documents

Reference	Title	Code
RD 1	ATBD Fundamental Climate Data Record of SSM/I Brightness Temperatures	SAF/CM/DWD/ATBD/ FCDR_SSMI/2.2
RD 2	ATBD Fundamental Climate Data Record of SSMIS Brightness Temperatures	SAF/CM/DWD/ATBD/ FCDR_SSMIS/2.2

## Table of Contents

I	Preface.....	5
1	The EUMETSAT SAF on Climate Monitoring .....	5
2	Introduction .....	6
II	SMMR .....	8
3	Algorithm Overview .....	8
3.1	The SMMR Instrument.....	8
3.2	Instrument operation.....	9
4	Algorithm Description .....	10
4.1	Data processing .....	10
4.1.1	Level 1B data processing.....	10
4.1.2	Level 1B geolocation .....	10
4.1.3	FCDR data processing.....	12
4.2	SMMR calibration.....	13
4.3	Applied corrections in Level 1B.....	15
4.3.1	Calibration offset adjustments.....	15
4.3.2	Correction for long-term drifts.....	15
4.3.3	Corrections for short-term drifts.....	16
4.3.4	Implementation.....	16
4.4	Applied corrections in FCDR.....	16
4.4.1	Along-scan correction .....	16
4.5	Computation of Brightness Temperatures .....	17
4.5.1	Spill-over correction.....	18
4.5.2	Polarization mixing.....	18
4.6	SMMR Instrument Homogenization.....	19
4.6.1	Inter-sensor calibration .....	19
4.7	Error Budget Estimates.....	22
4.7.1	Random Error.....	22


4.7.2	Systematic Error.....	23
4.8	Practical Considerations .....	25
4.8.1	Validation .....	25
4.8.2	Quality control .....	25
4.8.3	Outputs (FCDR Product Definition) .....	26
5	Assumptions and Limitations .....	26
6	References.....	28
7	Appendix A.....	30
8	Glossary.....	31
III	SSM/I .....	33
IV	SSMIS.....	33

## List of Tables

Table II-1: Nimbus-7 SMMR characteristics (Nimbus-7 Users Guide, Madrid et al. 1978).....	30
Table II-2: Antenna spill-over fractions $\delta$ and polarization mixing coefficients $Qv, Qh, \gamma v, \gamma h$ (from Njoku et al., 1998). .....	30
Table II-3: Summary of estimated systematic error source contributions. ....	30

## List of Figures

Figure II-1: Nimbus 7 Observatory (from Nimbus 7 Users Guide; Madrid, 1978). .....	9
Figure II-2: SMMR Instrument configuration (from Nimbus 7 Users Guide, 1978). ....	11
Figure II-3: SMMR schematic scan pattern (from Njoku et al., 1998).....	11
Figure II-4: SMMR FCDR processing flow chart. ....	13
Figure II-5: Scan angle dependent correction for the SMMR instruments. This image shows the along-scan correction at a common scene temperature of 200 K. Nadir is at position 24. ....	17
Figure II-6: Time series of monthly mean differences between observed and simulated SMMR TBs (left column) and SSM/I F08 TBs (right column). SMMR TBs are shown without inter-calibration and SSM/I TBs inter-calibrated to F11. Solid lines depict morning/midday orbits and dashed lines evening/midnight orbits. ....	20

	<b>Algorithm Theoretical Basis Document</b> <b>Microwave Imager Radiance FCDR R4</b> <b>SMMR Brightness Temperatures</b>	Doc. No: SAF/CMDWD/ATBD/FCDR_SMMR Issue: 2.3 Date: 2022-03-31
---	--	---

## I Preface

This document is structured in different logical parts, reflecting the different instrument series used to compile a Fundamental Climate Data Record (FCDR) from conical scanning microwave imagers. After a short introduction, summarizing the current status, the corresponding documents for the parts from the Special Sensor Microwave / Imager (SSM/I) and the Special Sensor Microwave Imager/Sounder (SSMIS) are referenced here. These parts are made available as separate documents. The main part of this document describes the methods to compile the Scanning Multichannel Microwave Radiometer (SMMR) component of the FCDR.


### 1 The EUMETSAT SAF on Climate Monitoring

The importance of climate monitoring with satellites was recognized in 2000 by EUMETSAT Member States when they amended the EUMETSAT Convention to affirm that the EUMETSAT mandate is also to “contribute to the operational monitoring of the climate and the detection of global climatic changes”. Following this, EUMETSAT established within its Satellite Application Facility (SAF) network a dedicated centre, the SAF on Climate Monitoring (CM SAF, <http://www.cmsaf.eu/>).

The consortium of CM SAF currently comprises the Deutscher Wetterdienst (DWD) as host institute, and the partners from the Royal Meteorological Institute of Belgium (RMIB), the Finnish Meteorological Institute (FMI), the Royal Meteorological Institute of the Netherlands (KNMI), the Swedish Meteorological and Hydrological Institute (SMHI), the Meteorological Service of Switzerland (MeteoSwiss), the Meteorological Service of the United Kingdom (UK MetOffice) and the Centre National de la Recherche Scientifique, Laboratoire d’études en Géophysique et Océanographie Spatiales, France (CNRS, LEGOS). Since the beginning in 1999, the EUMETSAT Satellite Application Facility on Climate Monitoring (CM SAF) has developed and will continue to develop capabilities for a sustained generation and provision of Climate Data Records (CDR’s) derived from operational meteorological satellites.

In particular the generation of long-term data sets is pursued. The ultimate aim is to make the resulting data sets suitable for the analysis of climate variability and potentially the detection of climate trends. CM SAF works in close collaboration with the EUMETSAT Central Facility and liaises with other satellite operators to advance the availability, quality and usability of Fundamental Climate Data Records (FCDRs) as defined by the Global Climate Observing System (GCOS). As a major task the CM SAF utilizes FCDRs to produce records of Essential Climate Variables (ECVs) as defined by GCOS. Thematically, the focus of CM SAF is on ECVs associated with the global energy and water cycle.

The CM SAF data sets can serve applications related to the new Global Framework of Climate Services initiated by the WMO World Climate Conference-3 in 2009. CM SAF is supporting climate services at national meteorological and hydrological services (NMHSs) with long-term data records but also with data sets produced close to real time that can be used to prepare monthly/annual updates of the state of the climate. Both types of products together allow for a consistent description of mean values, anomalies, variability, and potential trends for the

	<b>Algorithm Theoretical Basis Document</b> <b>Microwave Imager Radiance FCDR R4</b> <b>SMMR Brightness Temperatures</b>	Doc. No: SAF/CMDWD/ATBD/FCDR_SMMR Issue: 2.3 Date: 2022-03-31
---	--	---

chosen ECVs. CM SAF ECV data sets also serve the improvement of climate models both at global and regional scale.

A catalogue of all available CM SAF products is accessible via the CM SAF webpage, <http://www.cmsaf.eu/>. Here, detailed information about product ordering, add-on tools, sample programs and documentation is provided.

## 2 Introduction


This collection of CM SAF Algorithm Theoretical Basis Documents (ATBDs) provides information on the methods and the processing chain implemented for the CM SAF Fundamental Climate Data Record of brightness temperatures (TBs) from the SMMR, the SSM/I and the SSMIS. This fourth release is a continuation of the previous release (available from CM SAF; [http://dx.doi.org/10.5676/EUM\\_SAF\\_CM/FCDR\\_MWI/V003](http://dx.doi.org/10.5676/EUM_SAF_CM/FCDR_MWI/V003)).

Data from the space-borne microwave imagers and sounders such as the Scanning Multichannel Microwave Radiometer (SMMR), Special Sensor Microwave/Imager (SSM/I) and the Special Sensor Microwave Imager/Sounder (SSMIS) are used for a variety of applications, such as analyses of the hydrological cycle (precipitation and evaporation) and related atmospheric and surface parameters, as well as remote sensing of sea ice, soil moisture, and land surface temperatures. Carefully calibrated and homogenised radiance data sets are a fundamental prerequisite for climate analysis, climate monitoring and reanalysis. Several National Meteorological Services and Reanalysis centres assimilate microwave radiances directly and not derived geophysical parameters. Forecast and reanalysis can thus benefit from a Fundamental Climate Data Record (FCDR) of brightness temperatures (Poli et al. 2015). The generation of Thematic Climate Data Records (TCDRs) strongly relies on the availability of FCDRs. Highest possible TCDR quality can be achieved easiest in radiance space, in turn increasing the products value for users.

The predecessors of this data record and the data processor suite have originally been developed at the Max-Planck Institute for Meteorology (MPI-M) and the University of Hamburg (UHH) for the Hamburg Ocean Atmosphere Parameters and Fluxes from Satellite Data (HOAPS, <http://www.hoaps.org/>) climatology. HOAPS is a compilation of climate data records for analysing the water cycle components over the global oceans derived from satellite observation (Andersson et al. 2011). The main satellite instrument employed to retrieve the geophysical parameters is the SSM/I and much work has been invested to process and carefully homogenize all SSM/I instruments onboard the Defence Meteorological Satellite Program (DMSP) platforms F08, F10, F11, F13, F14 and F15 (Andersson et al., 2010).

The HOAPS processing suite has been transferred to CM SAF in a Research to Operations activity in order to provide a sustained processing of the climate data records which is one of the main tasks of CM SAF, but not in the focus of the research group at the MPI-M / UHH. The operational processing and reprocessing of the FCDRs and TCDRs as well as the provision to the research community is maintained and coordinated by the CM SAF.

The first release of the CM SAF FCDR (Fennig et al. 2013) focussed on the SSM/I series, covering the time period from 1987 to end of 2008. In order to continue the HOAPS TCDRs beyond 2008 it was necessary to extend the underlying FCDR of microwave TBs with the

	<b>Algorithm Theoretical Basis Document</b> <b>Microwave Imager Radiance FCDR R4</b> <b>SMMR Brightness Temperatures</b>	Doc. No: SAF/CMDWD/ATBD/FCDR_SMMR Issue: 2.3 Date: 2022-03-31
---	--	---

SSMIS sensor family aboard the DMSP platforms F16, F17, and F18, which was accomplished with the second release of the CM SAF FCDR (Fennig et al. 2015). This combined FCDR of SSM/I and SSMIS brightness temperatures provides a consistent FCDR from 1987 to 2013.

Following requests from users of the FCDR, the third release focussed on the extension of the microwave brightness temperature data record to the earlier time period from 1978 to 1987 with observations from the SMMR on-board Nimbus-7. However, this turned out to be a very challenging task, as it has not been possible to get hold of the original raw instrument data records. Although this data record must have eventually been transferred from the Marshall Space Flight Centre (MSFC) to the National Snow & Ice Data Center (NSIDC), it is currently not available from their archives. Instead, the Nimbus-7 SMMR Pathfinder Level 1B Brightness Temperatures data record, available from NSIDC (Njoku, 2003), is used to generate this FCDR.

This decision has important consequences to the corrections that can be derived, as it is not possible to undo the applied level 1B corrections and to restore the original antenna temperatures from the corrected brightness temperatures. Hence, observed differences and anomalies can not be reliably assigned to either insufficient corrections or undetected instrument deficiencies. Ideally all applied corrections should have been re-evaluated and only applied if a significant positive impact could be demonstrated. Nevertheless, the Pathfinder Level 1B Brightness Temperature data record is a major improvement over the original raw data record and the efforts to generate this data set is highly appreciated. Especially the ATBD (Njoku et al. 1998) is a valuable condensed source of information describing the various issues of the SMMR instrument on-board Nimbs-7.

The third release of the FCDR is described in Fennig et al. (2020) which also includes a decent overview of the applied methodologies.

With the 4<sup>th</sup> release of the Microwave Imager Radiance FCDR, the temporal coverage of the SSMIS has been extended to 31 December 2020 while the SMMR and SSM/I data records remain unchanged. The data records for the SSMIS sensors on-board F16, F17, and F18 have been reprocessed for this fourth FCDR release, implementing significant improvements.



## II SMMR

This part of the document focuses on the methods and procedures to process the level 1B Pathfinder SMMR data record to a FCDR. Although the SMMR consists of 10 channels, only the SSM/I like channels at 18 GHz, 37 GHz and 22 GHz (only vertically polarized) are inter-calibrated to the corresponding SSM/I channels of the reference instrument on-board DMSP F11. The other channels will be provided as part of the FCDR data files, but without inter-calibration.

### Summary of changes for release R4

A new bit is added to the scanline quality flag to indicate the reduced quality during the special operations period from April 3 to June 23, 1986 (see section 4.8.2).

## 3 Algorithm Overview

### 3.1 The SMMR Instrument

A detailed description of the SMMR is given in Gloersen and Barath (1977) and Madrid et al. (1978). Hence, only a short summary of essential information is given here.

Two SMMR instruments were operated on board Nimbus-7 and SEASAT. While only about three month of data from the SEASAT mission exist, the SMMR on Nimbus-7 delivered a data record covering nearly 8 years from October 25, 1978 until August 20, 1987.

The Nimbus-7 spacecraft operated in a sun-synchronous orbit with an inclination of 99° and an average altitude of 955 km. This configuration results in an orbital period of about 104 minutes and provided approximately 14 orbits per day. There are 8 instruments mounted on the observatory. Figure II-1 shows a diagram of the Nimbus-7 observatory and the locations of the instruments. The SMMR was mounted on the forward side in direction of flight. Due to power limitations only one instrument operated full time. The SMMR instrument operated most of the time on a 50% duty cycle: one day "on" followed by one day "off."

The SMMR was a ten-channel radiometer, measuring microwave radiation from the Earth's atmosphere and surface in five frequencies at vertical and horizontal polarization (see Table II-1). Six radiometers are integrated in the instrument, fed by one multispectral feedhorn. While the four radiometers operating at the lower frequencies (6.6 – 21 GHz) measure alternating polarizations each half-scan, the other two at 37 GHz measure continuously vertical and horizontal polarization. A schematic of the SMMR is shown in Figure II-2.

The instruments antenna consists of an offset parabolic reflector and the multi-frequency feed assembly. The reflector was mounted at a nadir angle of 42°, which results in an average Earth incidence angle (EIA) of 50.3°. The antenna rotates  $\pm 25^\circ$ , centred about the sub-satellite track, which results in a 780 km wide swath at the Earth's surface. The scan velocity varied sinusoidally, being fastest at 0° azimuthal scan angle and slowest at the scan edges. A complete scan was accomplished after 4.096 seconds. Cold space is used as the cold reference target, viewed directly through one of three cold-sky calibration horns. The warm calibration target is at the instruments ambient temperature.

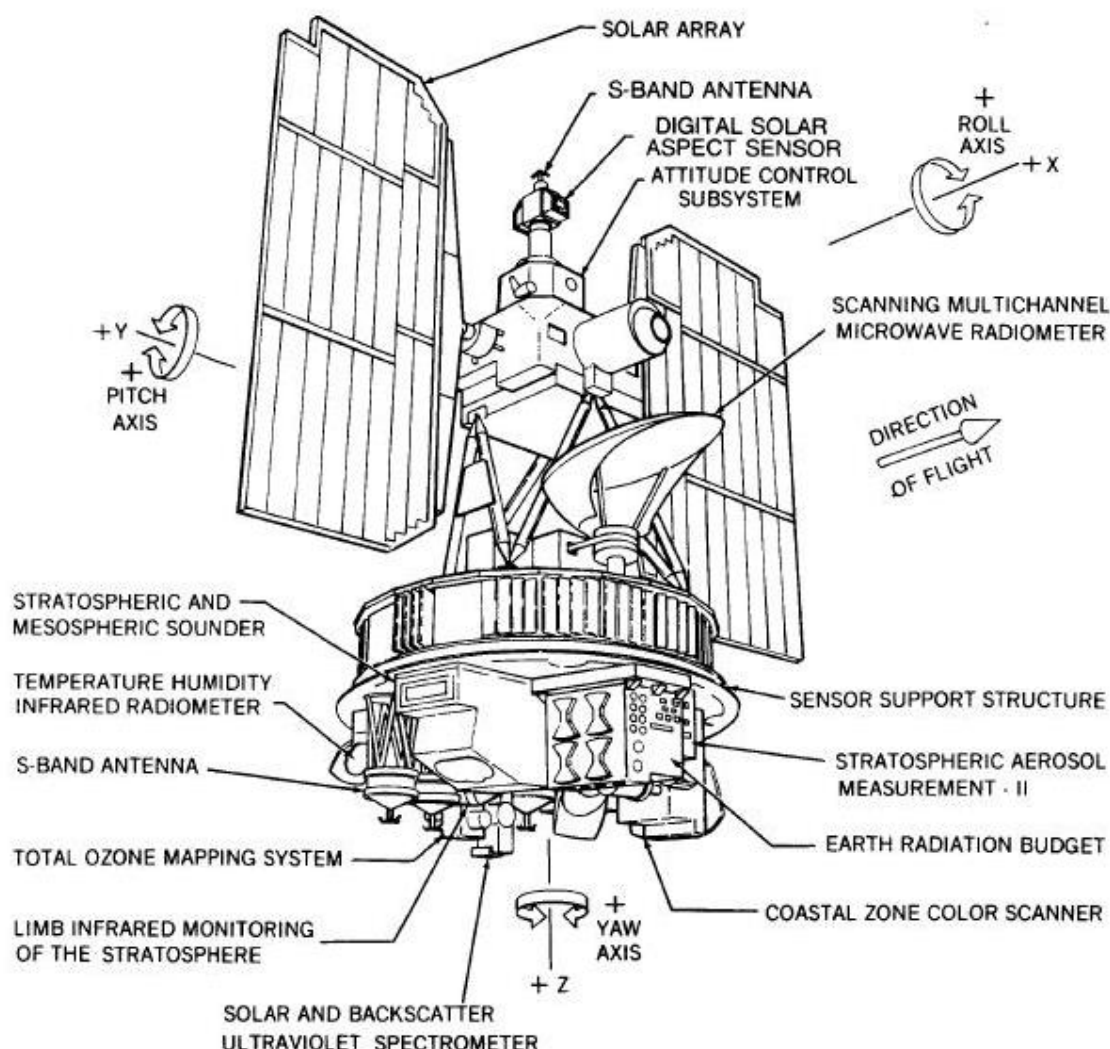


**Figure II-1:** Nimbus 7 Observatory (from Nimbus 7 Users Guide; Madrid, 1978).

### 3.2 Instrument operation

Acquisition of Nimbus-7 SMMR data commenced at midnight of October 25, 1978. The SMMR operated continuously during a three-week checkout period from start-up until November 16, 1978, at which time it began alternate-day operation. This was the normal mode of operation of the SMMR for most of its mission, as dictated by power sharing constraints among instruments on the spacecraft. Under normal operations the SMMR was turned on near midnight GMT (corresponding to a descending node equator crossing near 0° longitude) and turned off at approximately the same time the following day, in a continuing sequence. A special operations period occurred from April 3 to June 23, 1986, during which the SMMR was switched on and off more frequently, with "off" periods averaging 75 minutes and "on" periods averaging 30 minutes. The antenna scan mechanism was turned off permanently on August 20, 1987 for safety reasons, marking the end of the scanning SMMR data set (Njoku, 1998).

## 4 Algorithm Description

This section provides information on the processing of the level 1B data record and the processing chain implemented to compile the SMMR Fundamental Climate Data Record from the level 1B Pathfinder data record.

### 4.1 Data processing

#### 4.1.1 Level 1B data processing

A detailed description of the level 1B processing steps is given in Njoku et al. (1998) and summarized here for reference. The level 1B data processing was done in daily segments and all algorithms used for running averages (see section 4.2) were initialized at the beginning of the day. These are also re-initialized after data gaps longer than one minute. A quality status flag was generated for each scan to indicate potential quality losses. This quality flag is also copied to the final FCDR data record as *qc\_status*.

Inputs to the level 1B processor are level 1A antenna temperatures tapes (TAT). After reading and decoding, the radiometric calibration was done for each scanline (see section 4.2). This was followed by spill-over corrections (see section 4.5.1), absolute calibration correction (see section 4.3.1), as well as corrections for long-term (see section 4.3.2) and short-term drifts (see section 4.3.3). The resulting corrected antenna temperatures were then interpolated along and across scan lines to co-locate all channels to the 37 GHz FOV locations (see section 4.1.2). Finally the polarization mixing was corrected (see section 4.5.2) and the quality flags are assigned.

#### 4.1.2 Level 1B geolocation

The SMMR was observing the Earth surface with a reflector that scanned by oscillating about the vertical axis between azimuth angles of 25 degrees. Separate radiometers were used for vertical and horizontal polarizations only at 37 GHz. The channels at other frequencies used a single radiometer time-shared between vertical and horizontal polarizations. On the first half of each scan cycle (from right to left), these radiometers measured at vertical polarization while on the second half of the scan cycle (from left to right) horizontal polarization was measured (see Figure II-3). The 37 GHz vertical and horizontal polarizations were measured on both halves of the scan cycle. This original scan and FOV resolution is not provided in the level 1B data files. Instead all observations were interpolated to the 37 GHz positions with 47 scan positions for each half-scan. This geolocation remains unchanged in the FCDR data processing.

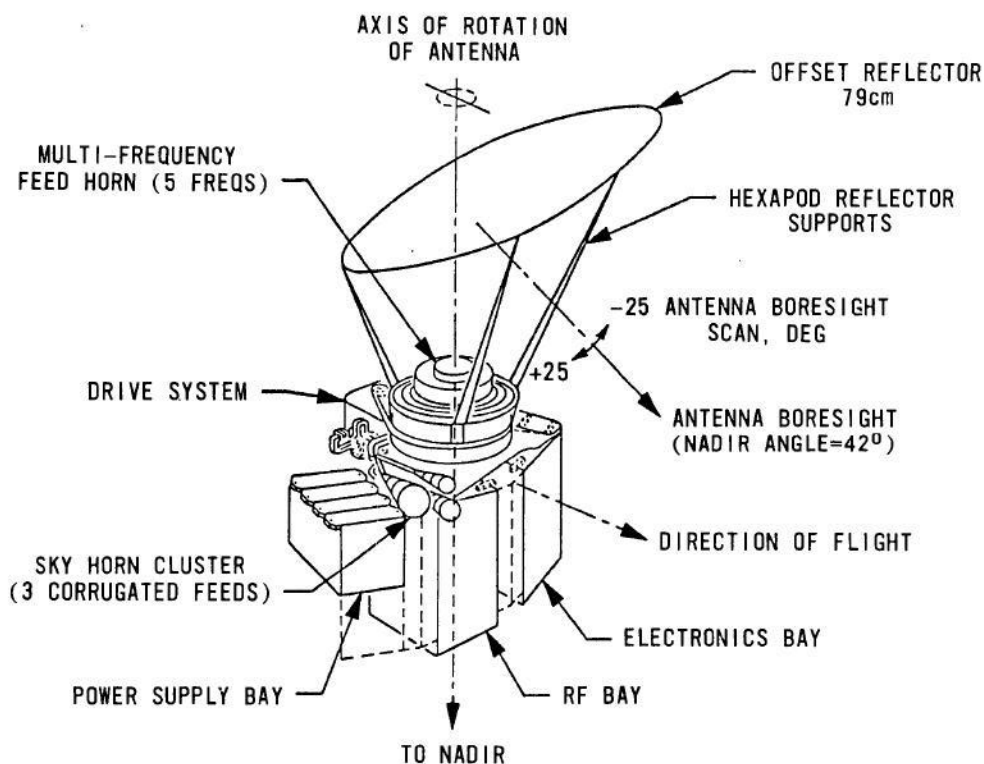


**Figure II-2:** SMMR Instrument configuration (from Nimbus 7 Users Guide, 1978).

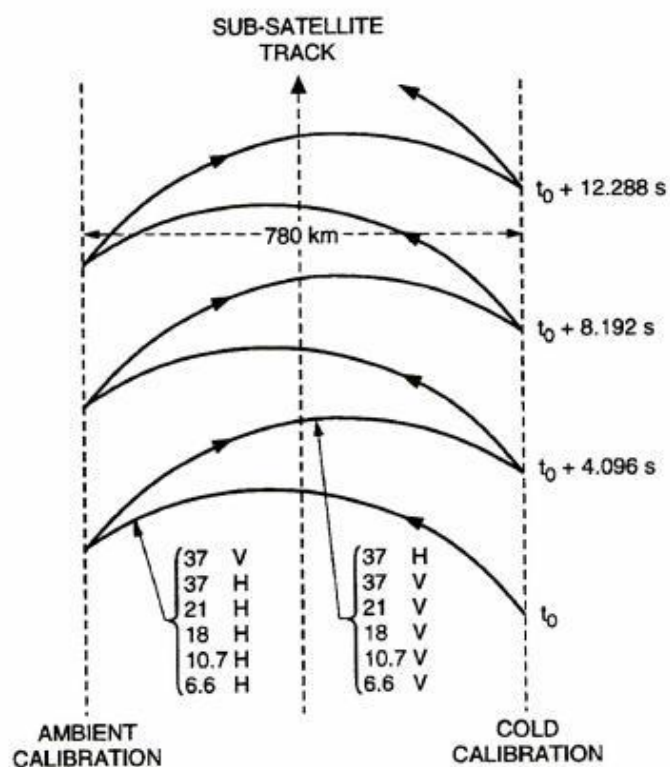


**Figure II-3:** SMMR schematic scan pattern (from Njoku et al., 1998).

#### 4.1.3 FCDR data processing

The SMMR FCDR data processing is split into two processing steps (see Figure II-4). During the first step, input data records are reformatted into the common FCDR data format. The level 1B data record is a collection of brightness temperature and instrument meta-data, archived as single orbit granules in HDF. These files contain all of the information from the original data files (see above). In order to further clean-up the data record, unique MD5 hash values are computed from the calibration data. The MD5 algorithm is a cryptographic hash function that takes a block of data and returns a unique fixed size hash value that can be used as a fingerprint to identify the data block and remove duplicate scans. All orbit granules for one day are filtered using the MD5 hash values. Valid scans are merged into daily SMMR FCDR NetCDF files. As the scan times are only available rounded to full seconds, the original time fraction is estimated with a linear regression fit using all scans from one day.

The spacecraft position is then used to fit the Simplified General Perturbations model SGP4 (Hoots and Roehrich, 1988) and to estimate daily Two-Line Element (TLE) sets. These TLE sets from the full data record are completed with TLE sets from <http://www.spacetrack.org/>, filtered and smoothed using a moving averaging window of  $\pm 7$  days to compile daily element sets for the entire data record period. A comparable method is used by Wentz (1991) to fit a simple orbit model. The geolocation is normally within 1 km of the original data and compared to time periods with available element sets.

In the following processing step, the new TLE sets are now used to predict the spacecraft position for each scan line. If the predicted and the archived position are offset by more than 6 km, the scan is marked in the *qc\_scan* quality flag with a geolocation error. Fractional revolution number and local azimuth angles (not available in the level 1B files) are computed using the predicted spacecraft position. Scan angles, reflected sun-footprint angles, and EIA are interpolated from 30 fixed positions per scanline to each of the 94 FOV full scan positions.

The attitude information (roll, pitch, yaw angles) is scanned for zero filled values and outliers. These angles were used without quality control in the level 1B processing to compute the EIAs. Errors in the EIA are mostly caused by anomalies in the attitude angles. Therefore the zero filled values and outliers in the attitudes angles and the EIA are replaced with interpolated values. However, no extrapolation is applied and incorrect values at the beginning or end of the files are set to undefined. The original quality flag *qc\_status* is unset accordingly in this case as the original flagging is no longer necessary due to the interpolation.

Finally the water/land surface type is assigned to each FOV (see section below). The uncorrected original calibration coefficients are re-computed with quality controlled data (see section 4.2) and the radiometer noise equivalent temperatures are estimated for each channel (see section 4.7.1). An along-scan correction is applied to the TBs (see section 4.4.1) to account for a non-uniformity of the measured brightness temperatures along the scan-line in the 37 GHz channels. Finally the inter-calibration offsets are computed (see section 4.6.1) and the final quality flags are assigned and global meta-data is defined.



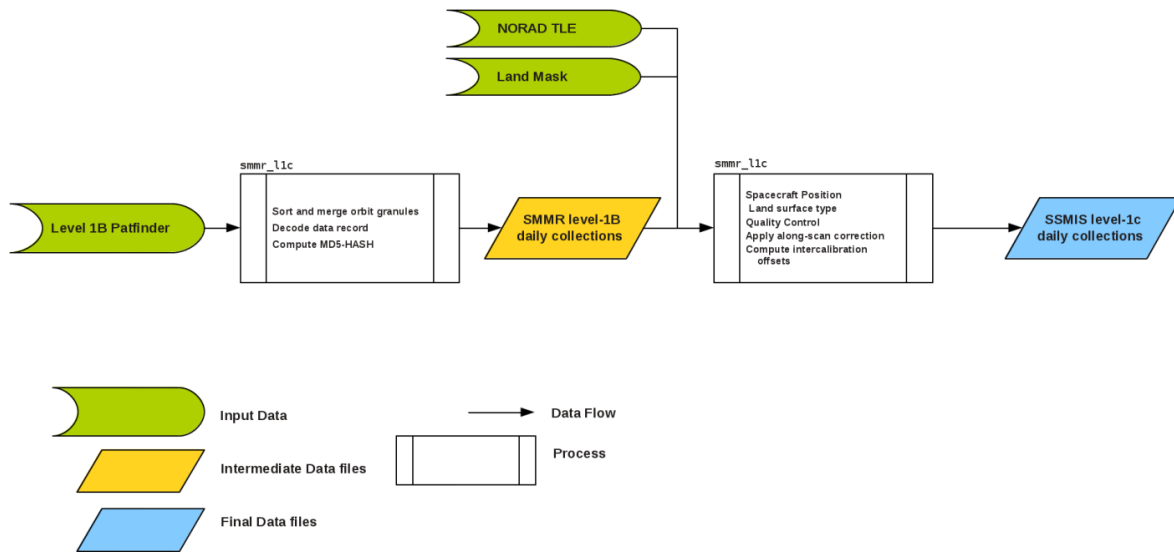


**Figure II-4:** SMMR FCDR processing flow chart.

#### a) Land-Sea mask

Each FOV is characterized with a surface type classification flag by the FCDR processor, using the CF-Metadata convention for flag variables (providing all information via the attributes *flag\_values* and *flag\_meanings*). Possible surface types are: water, land, and coast (for explanation see below). The centre latitude and longitude of the FOV is used to assign the surface type.

The SMMR specific land-sea mask is derived from the Global Land One-km Base Elevation data base (GLOBE, 1999). This data set is further adjusted to the footprint resolution by first removing small islands and landmasses with a diameter of less than 5 km, treating these areas as open water. These thresholds are based on the experience with the HOAPS precipitation algorithm, which is sensitive to land influence. This provides the basic land-sea classification. In a second step the coastal areas are defined by expanding the remaining land areas 50 km into the sea. Due to the large footprint size of the 6.6 and 10 GHz channels (see Table II-1), this surface type classification is only appropriate for the channels from 18 GHz to 37 GHz.

## 4.2 SMMR calibration

The basic underlying assumption for the SMMR calibration is a linear relation of the radiometer output voltage (measured in counts  $C$ ) to the radiometric input. In this case two reference targets with known temperatures and corresponding radiometer measurements are sufficient for an absolute linear two-point calibration. The calibration method used in the level 1B data record is taken from the SMMR CELL data record (Fu et al., 1988):

$$T_A = I + S \cdot \left( \frac{C_A - C_H}{C_C - C_H} \right), \quad \text{Equation II-1}$$

where  $T_A$  is the antenna temperature,  $C_A$ ,  $C_H$ , and  $C_C$  are the measured counts when the radiometer is switched to the antenna, the warm load calibration, and cold load calibration, respectively. The calibration coefficients  $S$  and  $I$  are functions of the instruments component temperatures:

$$\begin{aligned} I &= a_1 + a_2 T_{sw} - \Delta_{FH} \\ S &= a_3 (T_{sw} - 2.7) + \Delta_{CH} \end{aligned} \quad \text{Equation II-2}$$

The  $\Delta_{FH}$  term is a correction for temperature gradients from the multi-frequency feedhorn along the feedhorn waveguide to the receiver and is given by:

$$\Delta_{FH} = (T_{sw} - T_{FH}) - \left( \frac{T_{FW} - T_{FH}}{\alpha_1} \right) + \left( \frac{T_{sw} - T_{FW}}{\alpha_1 \beta_1} \right), \quad \text{Equation II-3}$$

with  $T_{sw}$ ,  $T_{FH}$ , and  $T_{FW}$  are the Dicke switch, feedhorn, and feedhorn waveguide temperatures, respectively.

The  $\Delta_{CH}$  term is a correction for temperature gradients from the cold-sky calibration horn along the calibration horn waveguide to the receiver and is given by:

$$\Delta_{CH} = (T_{sw} - T_{CH}) - \left( \frac{T_{CW} - T_{CH}}{\alpha_2} \right) + \left( \frac{T_{sw} - T_{CW}}{\alpha_2 \beta_2} \right), \quad \text{Equation II-4}$$

with  $T_{CH}$ , and  $T_{CW}$  are the calibration horn and calibration horn waveguide temperatures. The calibration coefficients  $a_{1,2,3}$ ,  $\alpha_{1,2}$ , and  $\beta_{1,2}$  are given in Njoku et al. (1998).

The warm calibration target of the SMMR is the internal ambient temperature at ~300 K. The cold reference target is the cold space viewed with three calibration horns (dependent on frequency). The cold sky is assumed to be at a constant temperature of 2.7 K, i.e. cosmic background temperature. The radiometer views the internal warm and cold calibration targets once during a scan rotation. The warm calibration readings are sampled at the left end of the oscillating scan and the cold calibration readings at the right end (see Figure II-3). The instrument temperatures are sampled every eight scans using platinum resistance thermistors and are embedded in the data record.

In order to reduce the noise, calibration warm and cold counts are smoothed in the level 1B data processing using a running one-sided average:

$$\bar{C}(s) = w \cdot C(s) + (1 - w) \cdot \bar{C}(s - 1), \quad \text{Equation II-5}$$

with  $s$  as the scanline number,  $w$  as the weight of the new data value and  $\bar{C}$  as the smoothed count. A weight of  $w = 0.1$  was chosen as a compromise between noise reduction and overdamping. Hence 90% of the information on the counts for a given scanline (and hence associated estimate of the gain) comes from the previous scanlines.

Also the instrument temperatures are averaged using the same method. As these temperatures are only available every eight scans, a weight of  $w = 0.6$  was used.

The calibration coefficients  $S$  and  $I$  are not available in the level 1B data records. In order to complete the data record and to estimate the instrument noise level (see section 4.7.1), these coefficients are re-calculated using equations II-2 and II-5 and then archived in the FCDR data files for reference.

### 4.3 Applied corrections in Level 1B

In the level 1B processing, corrections for absolute calibration, long-term drifts, short-term drifts, and polarization mixing are applied. The polarization mixing decoupling is treated as part of the antenna pattern correction and described in section 4.5.2. The level 1B corrections applied to the antenna temperatures are explained in detail in Njoku et al. (1998) and summarized below.

#### 4.3.1 Calibration offset adjustments

A two-point linear absolute calibration adjustment to the SMMR data record was estimated using ocean areas acting as the cold calibration target and the internal ambient instrument warm load as the warm calibration target. The coefficients were derived over calm, cloud-free oceanic areas, characterized by low emissivity values. Modelled brightness temperatures were compared to the observed SMMR brightness temperatures to derive a linear calibration adjustment to the antenna temperatures:

$$T'_{Acorr} = a + b \cdot T'_A, \quad \text{Equation II-6}$$

where  $T'_A$  is the normalized SMMR antenna temperature (after spill-over correction) from equation II-10,  $T'_{Acorr}$  is the corrected value, and  $a$ ,  $b$  are the linear calibration adjustment coefficients. The calibration constraints can be written as:

$$\begin{aligned} T_{Bm} &= T_{Bcorr}^o = a + b \cdot T_B^o, \\ I' &= a + b \cdot I' \end{aligned} \quad \text{Equation II-7}$$

where  $T_B^o$  is the mean observed SMMR brightness temperature for the cold calibration target and  $T_{Bm}$  is the corresponding modelled brightness temperature. Solving these equations for the coefficients  $a$  and  $b$  yields:


$$\begin{aligned} a &= I' \cdot \frac{(T_{Bm} - T_B^o)}{(I' - T_B^o)} \\ b &= \frac{(I' - T_{Bm})}{(I' - T_B^o)} \end{aligned} \quad \text{Equation II-8}$$

The calibration correction coefficients  $a$  and  $b$  depend on the warm load equivalent brightness  $I'$  and are updated online for each new set of calibration data. The values for  $T_{Bm}$  and  $T_B^o$  are given in Njoku et al. (1998).

#### 4.3.2 Correction for long-term drifts

Aging of the radiometer components can lead to a slow but steady degradation in the radiometer performance. Long-term drifts in the SMMR data records have been studied by Francis (1987) and Gloersen et al. (1992). The basic method used by the authors was to analyse temporal variations in the global mean brightness temperatures over oceanic regions, assuming that the geophysical parameters are constant over time. Njoku et al. (1998) followed this method and studied the long-term evolution of the mean brightness temperatures in all SMMR channels. The largest drift was found for the 21h channel with an increase of 36 K until March 1985 when it was turned off. The observed drifts are corrected in the level 1B data record using a polynomial fit of the globally averaged antenna temperatures, after removing



	<b>Algorithm Theoretical Basis Document</b> <b>Microwave Imager Radiance FCDR R4</b> <b>SMMR Brightness Temperatures</b>	Doc. No: SAF/CMDWD/ATBD/FCDR_SMMR Issue: 2.3 Date: 2022-03-31
---	--	---

mean seasonal cycle variations. The polarization mixing was not corrected for in order to keep the signals from each radiometer independent at this stage. Otherwise the strong drift in the 21h channels would have been mixed into the 21v channel.

#### 4.3.3 Corrections for short-term drifts

Orbit dependent solar illumination of the instrument can affect the radiometric calibration. Although temperature gradients are accounted for in the calibration equation II-1, not all effects might be compensated accurately. Especially when the spacecraft leaves or enters the Earth's shadow, strong temperature gradients can be observed, possibly leading to un-modelled thermal emissions in the wave guides and switches of the instrument (Francis, 1987).

To correct for this type of errors, orbit dependent corrections were derived following a method described by Francis (1987). Mean brightness temperature differences between ascending and descending orbits were analysed to derive brightness temperature drift corrections as a function of the spacecraft ecliptic angle. The corrections are derived for each year and then linearly interpolated to the observation time. Unfortunately, the values are not available in Njoku (1998).

#### 4.3.4 Implementation

The corrections for long-term drifts  $T_{lt}$  and short-term drifts  $T_{st}$  were incorporated into the calibration by replacing the coefficients in equation II-8 with:

$$\begin{aligned}
 a_{new} &= I' \cdot \frac{(T_{Bm} - T_{lt} - T_{st} - T_B^0)}{(I' - T_B^0)} \\
 b_{new} &= \frac{(I' + T_{lt} + T_{st} - T_{Bm})}{(I' - T_B^0)} \cdot
 \end{aligned}
 \quad \text{Equation II-9}$$

As the original coefficients  $a_{new}$  and  $b_{new}$  are not available in the data records and the short-term correction are not available in Njoku et al. (1998), it is not possible to undo the applied corrections and to revert the original antenna temperatures. Therefore, any other additional correction must be done on top of the already applied level 1B corrections.

### 4.4 Applied corrections in FCDR

#### 4.4.1 Along-scan correction

A general along-scan non-uniformity of the SMMR antenna temperatures is to be expected, caused by the cross-polarization coupling (see section 4.5.2). Although most of this effect is removed by the applied scan-position dependent polarization mixing correction, significant variations in the final TBs can remain. To analyse these, the match-up dataset with modelled brightness temperatures (see section 4.6.1) has been used here.

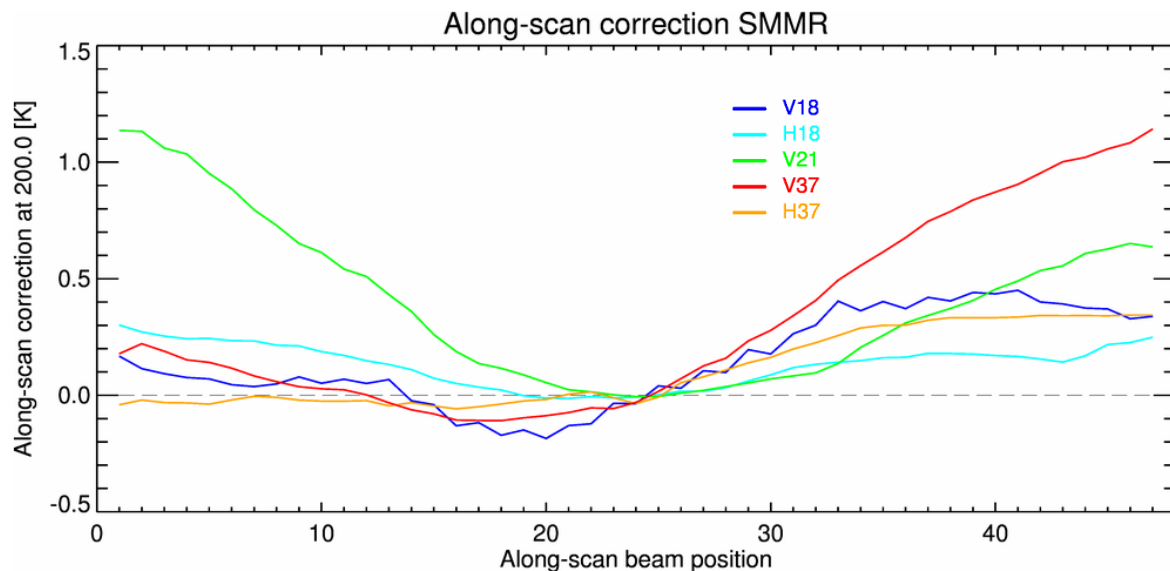


**Figure II-5:** Scan angle dependent correction for the SMMR instruments. This image shows the along-scan correction at a common scene temperature of 200 K. Nadir is at position 24.

Differences between observed and modelled brightness temperatures for each channel with surface type sea between 50°S and 50°N are averaged into FOV-position bins for the complete SMMR time period at 10-daily intervals. Then a factor at each FOV position is computed as the ratio of the position averaged value to the unaffected FOVs at the scan line centre. The time mean results are shown in Figure II-5 for a nominal scene temperature at 200 K. Most pronounced features are the large offsets of about 1 K in the 21v channel on the left scan side and in the 37v channel on the right scan side. The other channels show small offsets on the left side (0-0.3 K) and small but a little larger offsets at the right side (0.2-0.5 K). The large differences in the 21v channel are not constant over time and are most likely caused by the polarization mixing from the problematic 21h channel. The 21h channel depicts a strong trend and degradation with time, which can not be removed completely by the long-term drift corrections and polarization mixing decoupling procedure. Also the observed differences in the 18 GHz channels are not constant over time, but do show a seasonal variation with smaller offsets in northern hemisphere winter and larger offsets in northern hemisphere summer months. Only the deviations in the 37 GHz channels are constant over time.

Following these results, only the along-scan biases in the 37 GHz channels are corrected. As the differences in the vertical polarization are much larger than in the horizontal polarization, the cross-polarization is assumed to be zero and the bias correction reduces to a scan position depended factor.

#### 4.5 Computation of Brightness Temperatures

The antenna temperature is a direct measure of the radiation entering the antenna feedhorn. It may be expressed in terms of an integral of the scene brightness temperature distribution incident on the antenna reflector and the effective co- and cross-polarized far-field antenna power patterns. To obtain an estimate of brightness temperature TB from TA it is necessary to

apply an Antenna Pattern Correction (APC) to account for cross-polarization mixing  $\chi_{v,h}$  and feedhorn spill-over loss  $\delta$ .

#### 4.5.1 Spill-over correction

The SMMR has low antenna beam efficiencies. As a result of this, there are significant contributions from the antenna side-lobes in addition to the main lobe. It is assumed that these view the cosmic background at 2.7 K. The correction for the fraction of cold space that enters the side-lobes is applied in the level 1B data record as follows:

$$T'_{Ap} = \frac{T_{Ap} - 2.7\delta_p}{1 - \delta_p}, \quad \text{Equation II-10}$$

where  $T'_{Ap}$  are the normalized antenna temperatures for polarization  $p$ ,  $\delta_p$  are the frequency dependent spill-over fractions (see Table II-2), and  $T_{Ap}$  is the antenna temperature derived with the calibration equation II-1.

#### 4.5.2 Polarization mixing

Additional to the expected internal cross-polarization leakage at the polarization selector switches, large polarization mixing is induced as a result of the instruments design. The antenna system consists of a scanning parabolic reflector and a fixed multispectral feedhorn. Due to the antenna oscillating rotation, the alignment of the antenna pattern polarization vector relative to the Earth surface changes with increasing scan angle  $\varphi$ . With increasing scan angle, vertical polarization is mixed into horizontal polarization and vice versa. This effect is zero at the centre of the scan-line. Several studies (Gloersen et al. 1980, Gloersen 1987, Francis 1987) addressed this problem. The procedure implemented in the level 1B data records (Njoku et al., 1989) to correct for this effect follows that of Gloersen (1987).

The scan angle dependent integration of the antenna pattern over the antenna FOV can be approximated by:

$$\begin{aligned} T'_{Av}(\varphi) &= (1 - \chi_v(\varphi)) \cdot T_{Bv} + \chi_v(\varphi) \cdot T_{Bh} \\ T'_{Ah}(\varphi) &= (1 - \chi_h(\varphi)) \cdot T_{Bh} + \chi_h(\varphi) \cdot T_{Bv} \end{aligned} \quad \text{Equation II-11}$$

where  $\varphi$  is the azimuthal scan angle,  $\chi_{v,h}(\varphi)$  are derived by integrating the normalized antenna patterns, and  $T_{Bv,h}$  are the respective brightness temperatures.

The  $\chi_{v,h}(\varphi)$  have  $\sin^2(\varphi)$  dependence:

$$\begin{aligned} \chi_v(\varphi) &= Q_v \cdot \sin^2(\varphi - \gamma_v) \\ \chi_h(\varphi) &= Q_h \cdot \sin^2(\varphi - \gamma_h) \end{aligned} \quad \text{Equation II-12}$$

where  $Q_v, Q_h, \gamma_v, \gamma_h$  are the amplitudes and phase shifts of the polarization mixing. It was found that pre-launch antenna-pattern measurements are insufficient to correctly determine these coefficients. Therefore they are estimated empirically from in-orbit data, fitting equation II-12 with time-averaged observations over oceanic regions. The final set of coefficients is given in Table II-2. Equation II-11 is then inverted to compute the scene brightness temperatures from the normalized antenna temperatures:

$$\begin{aligned}
T_{Bv}(\varphi) &= \frac{1-\chi_h(\varphi)}{1-\chi_v(\varphi)-\chi_h(\varphi)} \cdot T'_{Av} + \frac{\chi_v(\varphi)}{1-\chi_v(\varphi)-\chi_h(\varphi)} \cdot T'_{Ah} \\
T_{Bh}(\varphi) &= \frac{1-\chi_v(\varphi)}{1-\chi_v(\varphi)-\chi_h(\varphi)} \cdot T'_{Ah} + \frac{\chi_h(\varphi)}{1-\chi_v(\varphi)-\chi_h(\varphi)} \cdot T'_{Av}
\end{aligned}$$

**Equation II-13**

## 4.6 SMMR Instrument Homogenization

### 4.6.1 Inter-sensor calibration

In order to ensure a homogeneous time series of brightness temperatures from the SMMR across the SSM/I to the SSMIS sensors, the varying individual instrument characteristics have to be corrected by an inter-sensor calibration of the individual radiometers. The inter-calibration reference selected for the CM SAF FCDR is the SSM/I on-board DMSP F11 [RD 1]. Because the SMMR does not have a temporal overlap with F11, it is inter-calibrated to the corrected F08 radiometer, used as a transfer standard. However, the overlap period of SMMR and SSM/I F08 is just about one month. This is not a sufficient record length to derive stable inter-calibration coefficients as seasonal or other multi-monthly variations can not be accounted for. It is therefore not possible to use the statistical methods developed for SSM/I and SSMIS inter-calibration [RD 1, RD 2]. Instead, a double-difference technique against modelled brightness temperatures from reanalysis profiles is employed here (Sapiano, 2013).

It is important to keep in mind that this inter-calibration is not intended to completely remove all observed differences. Instead the measured SMMR brightness temperatures are corrected to be physically consistent with corresponding SSM/I brightness temperatures. This means small differences due to different nominal channel centre frequencies (e.g. 18 GHz and 19 GHz) and bandwidths are to be expected. Also the different incidence angles of the measurements will result in overall and time-varying differences. These must not only be accounted for during the inter-calibration in order to derive physically consistent inter-calibration coefficients but also later on in the application. This can be done either directly in the algorithm or indirectly by normalizing the observed TBs to a nominal frequency and EIA.

Using a reanalysis as a transfer standard has advantages but also limitations. Firstly, the most important requirement here is the temporal stability of the reanalysis. This is the basic underlying assumption to allow a transfer of an observed bias from the SSM/I time period to the SMMR time period. Secondly, the uncertainties in the applied radiative transfer model and the emissivity model should be well behaved in order to cancel out in the double difference technique. However, using reanalysis might induce uncertainty due to incorrect representation of diurnal cycles.

While using modelled brightness temperatures for the inter-calibration, the EIA dependence of the brightness temperatures and the frequency shifts are explicitly accounted for and the observed TBs must not be normalized beforehand. Also the different equator overpass times of Nimbus-7 (12 AM) and DMSP F08 (6 AM) are considered by the temporal collocation criterion. However, a serious limitation is the large uncertainty of surface emissivity models over land, ice and snow covered surfaces due to unknown surface emissivities. Also the strong diurnal cycle over land is not resolved by the reanalysis time steps. Additionally, rainy and cloudy scenes increase the uncertainty of the radiative transfer model due to scattering effects

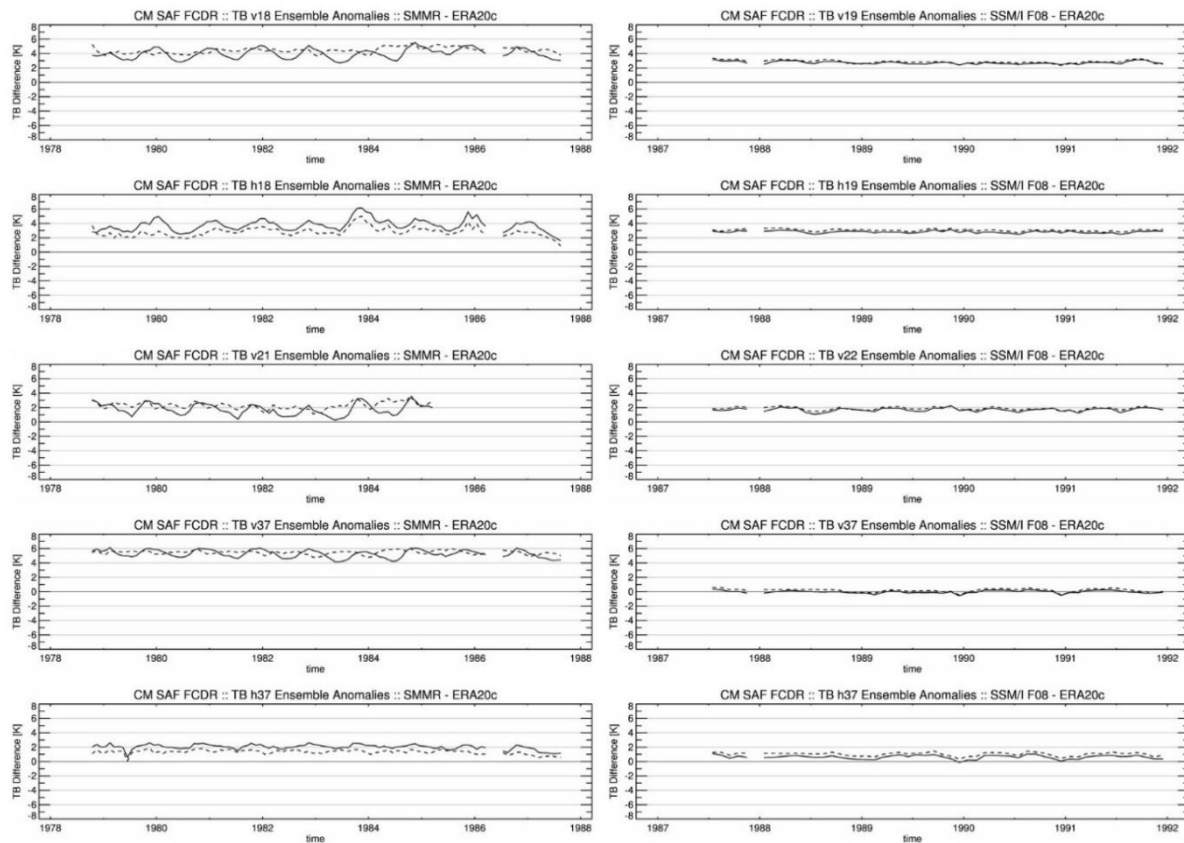


**Figure II-6:** Time series of monthly mean differences between observed and simulated SMMR TBs (left column) and SSM/I F08 TBs (right column). SMMR TBs are shown without inter-calibration and SSM/I TBs inter-calibrated to F11. Solid lines depict morning/midday orbits and dashed lines evening/midnight orbits.

of the water droplets. In order to minimize these influences, only cloud-free and lightly cloudy scenes over water surfaces are selected for the inter-calibration match-up data sets.

The profile and surface data used here are taken from the ERA-20C reanalysis (Poli et al. 2013). Brightness temperatures at the top of the atmosphere are calculated with RTTOV 11.2 (Saunders et al. 2013) and the surface emissivity with FASTEM 6 (Meunier et al. 2014). Profiles from ERA20c are available every 3 hours, resulting in maximum time differences of 90 minutes between observed and simulated brightness temperatures.

The simulations are done for the entire time period covered by the non-intercalibrated SMMR and the SSM/I FCDR for F08. In order to reduce the uncertainty in the observed differences, the match-up data is gridded into daily global  $1^\circ$  equal angle grids, separately for ascending and descending orbits. Global monthly mean differences between simulated and observed brightness temperatures for all inter-calibrated channels are shown in Figure II-6. No significant trends can be observed for the SSM/I TBs. As ERA20c does not include satellite observations, this likely assures that the global mean brightness temperatures in both independent data sets, SSM/I FCDR and ERA-20C, are stable over the selected time period. Morning and evening TB anomalies depict nearly identical temporal variations and agree to within 0.2 K in the mean value. Only the 37h channel shows a larger difference with a value of 0.4 K between ascending and descending orbits. This also underlines the stability and quality of the SSM/I FCDR.

The SMMR anomalies show a different behaviour. Generally they are stable over time despite the last months of 1987 where the differences get smaller in all channels. The 21v channel seems to be affected by a small upward drift towards the end of its lifetime (1983-1985). These trends are most likely caused by the correction of the long-term trend in the level 1B data record (see section 4.3.2). As this correction was derived from a polynomial fit of the absolute global mean values, existing natural climate trends could have been not accounted for. Also seasonal variations of the ascending and descending orbits can be observed, which do not agree. Phase shifts in the anomalies are visible for 18v, 21v, 37v, and 37h while the amplitude of the variations decreases with increasing frequency from about 2 K to 0.5 K.

It was not possible to identify the root cause for these temporal variations and offsets. The magnitude of the observed TB anomalies and their overall decrease with frequency might be caused by unresolved variations in the Earth incidence angle. This can be either due to errors in the satellite attitude control or deficiencies in the applied short-term, orbit angle dependent, correction in the level 1B data (see section 4.3.3). These were derived by forcing ascending minus descending TB differences to be zero without accounting for the different EIA values at ascending and descending paths or diurnal variations. As this level 1B correction is based on look-up tables, which are not available, it can not be reverted. Hence, it is not possible to separate the effects and identify the physical reasons for the observed seasonal variations.

The inter-calibration model used for this FCDR is adapted from the absolute calibration correction applied in the level 1B data processing (see section 4.3.1). This correction is a scene dependent correction to a modelled background acting as cold target while keeping the warm target at the instrument warm load reference temperature. A simple TB offset would therefore result in scene dependent biases at warm scene temperatures.

The cold target for the FCDR is now defined as the inter-calibrated mean brightness temperature. This correction is done by applying the derived double-differences to inter-calibrate the SMMR TBs to the F08 reference sensor. Keeping the nomenclature from Njoku et al. (1989), a linear correction is then defined as:

$$T_B^{ic} = c + d \cdot T_B, \quad \text{Equation II-14}$$


where  $T_B$  is the observed SMMR brightness temperature,  $T_B^{ic}$  is the inter-calibrated value and  $c$  and  $d$  are the inter-calibration coefficients. The constraints for the match-up dataset can be written as:

$$\begin{aligned} T_B^c &= T_B^o + (T_{Bm} - T_B^o) - (T_{Bm}^{\#} - T_B^{\#o}) \\ T_B^c &= c + d \cdot T_B^o \\ I' &= c + d \cdot I' \end{aligned}, \quad \text{Equation II-15}$$

where  $T_B^c$  is the mean corrected SMMR brightness temperature,  $T_B^o$  is the mean observed SMMR brightness temperature,  $(T_{Bm} - T_B^o)$  is the mean SMMR brightness temperature difference to the modelled TB,  $(T_{Bm}^{\#} - T_B^{\#o})$  is the corresponding mean SSM/I brightness temperature difference and  $I'$  is the normalized warm load reference brightness. These equations are solved to give the following values for  $c$  and  $d$ :

$$\begin{aligned} c &= I' \cdot \frac{(T_B^c - T_B^o)}{(I' - T_B^o)} \\ d &= \frac{(I' - T_B^c)}{(I' - T_B^o)}. \end{aligned} \quad \text{Equation II-16}$$



	<b>Algorithm Theoretical Basis Document</b> <b>Microwave Imager Radiance FCDR R4</b> <b>SMMR Brightness Temperatures</b>	Doc. No: SAF/CMDWD/ATBD/FCDR_SMMR Issue: 2.3 Date: 2022-03-31
---	--	---

The coefficients  $c$  and  $d$  depend on the warm load equivalent brightness  $I'$  and are updated online for each new set of calibration data. The inter-calibration offsets  $\Delta T_{ICAL}$  to the brightness temperatures are assumed to be valid over all surface types and computed during the final processing for each FOV and then separately archived in the SMMR FCDR data files:

$$\Delta T_{ICAL} = T_B^{ic} - T_B. \quad \text{Equation II-17}$$

By keeping the inter-calibration TB offsets separately from the TBs itself, each user has the freedom to choose whether to apply the correction or use the uncorrected values within their application.

## 4.7 Error Budget Estimates

A complete error analysis for the SMMR brightness temperatures is not feasible as it requires careful and fully documented pre-launch measurements of all components, subsystems and of the final fully integrated system simulating expected orbital conditions. However, not all information about the instrument is available. Also it is known, that the pre-launch measurements are not complete and some are of questionable value (Gloersen, 1987). Therefore, only an estimate of the expected error budget and the contributing terms can be derived. Unknown values are taken from the SSM/I uncertainty estimation (RD 1).

The total expected error of a quantity can be divided into two components: a systematic error (accuracy) and a random error (precision). While the random error of the TBs can be determined in-orbit from the instrument measurements used to calibrate the radiometer, the total systematic error must be identified during the ground measurements. Following the ISO Guide to the expression of uncertainties (ISO GUM) the random errors can be evaluated by statistical methods and are therefore Type A uncertainties. The systematic errors must be estimated from prelaunch measurements or validation activities and thus are Type B uncertainties.

### 4.7.1 Random Error

The precision of a radiometer is usually expressed as a noise equivalent temperature  $NE\Delta T$ , which is the standard uncertainty of the measurement. This uncertainty is defined as the standard deviation of the radiometer referenced to the energy of the radiation incident on the antenna. This noise can be estimated using the SMMR in-orbit calibration measurements and the calibration equation (see also section 4.2). Applying standard error propagation to equation II-1 yields:

$$NE\Delta T = \sqrt{U(I)^2 + U(S)^2 + U(\overline{C_H})^2 + U(\overline{C_C})^2 + U(\overline{C_A})^2}$$

$$NE\Delta T = \sqrt{\left(\frac{\delta T_A}{\delta I} \cdot \sigma_I\right)^2 + \left(\frac{\delta T_A}{\delta S} \cdot \sigma_S\right)^2 + \left(\frac{\delta T_A}{\delta C_H} \cdot \sigma_{C_H}\right)^2 + \left(\frac{\delta T_A}{\delta C_C} \cdot \sigma_{C_C}\right)^2 + \left(\frac{\delta T_A}{\delta C_A} \cdot \sigma_{C_A}\right)^2}, \quad \text{Equation II-18}$$

with the following standard uncertainties contributing to the combined standard variability:

- Standard uncertainty due to noise in the calibration offset coefficient  $\sigma_I$ :

$$U(I) = \frac{\delta T_A}{\delta I} \cdot \sigma_I = \left[ S \cdot \left( \frac{C_A - C_H}{C_C - C_H} \right) \right] \cdot \sigma_I , \quad \text{Equation II-19}$$

- Standard uncertainty due to noise in the calibration slope coefficient  $\sigma_S$ :

$$U(S) = \frac{\delta T_A}{\delta S} \cdot \sigma_S = \left[ \frac{C_A - C_H}{C_C - C_H} \right] \cdot \sigma_S , \quad \text{Equation II-20}$$

- Standard uncertainty due to noise in the averaged hot counts  $\sigma_{\overline{C_H}}$ :

$$U(\overline{C_H}) = \frac{\delta T_A}{\delta \overline{C_H}} \cdot \sigma_{\overline{C_H}} = \left[ S \cdot \left( \frac{C_A - C_C}{(C_C - C_H)^2} \right) \right] \cdot \sigma_{\overline{C_H}} , \quad \text{Equation II-21}$$

- Standard uncertainty due to noise in the averaged cold counts  $\sigma_{\overline{C_C}}$ :

$$U(\overline{C_C}) = \frac{\delta T_A}{\delta \overline{C_C}} \cdot \sigma_{\overline{C_C}} = \left[ S \cdot \left( \frac{C_H - C_A}{(C_C - C_H)^2} \right) \right] \cdot \sigma_{\overline{C_C}} , \quad \text{Equation II-22}$$

- Standard uncertainty due to noise in the antenna counts  $\sigma_A$ :

$$U(C_A) = \frac{\delta T_A}{\delta C_A} \cdot \sigma_{C_A} = \left[ S \cdot \left( \frac{1}{C_C - C_H} \right) \right] \cdot \sigma_{C_A} . \quad \text{Equation II-23}$$

The standard deviations of the smoothed cold counts, smoothed hot counts and smoothed calibration coefficients are estimated from all available valid observations on a daily basis. The daily mean noise equivalent temperature  $NE\Delta T$  for each channel can then be estimated while viewing the cold target, i.e. replacing  $C_A$  with  $C_C$ . As the variability of the SMMR cold counts is larger than the variability of the warm counts, this value is a valid estimate for the maximum expected  $NE\Delta T$ .


The estimated variances of the smoothed cold counts, smoothed hot counts, calibration coefficients, and the noise equivalent temperature are archived in the FCDR data files as daily mean values.

#### 4.7.2 Systematic Error

As noted above, it is not possible to specify a complete systematic error for the SMMR brightness temperatures. According to the instrument specifications, the absolute uncertainty is  $< 2$  K (Madrid et al. 1978). Apart from the aforementioned limitations to trace observed systematic differences back to SI standards, there is a more general problem in obtaining an accurate standard for comparison with the SMMR observations. There are no absolute reference observations available to validate the absolute calibration because the SMMR is a unique observing system. This means the brightness temperatures can only be compared against similar observations, for example aircraft measurements with a similar radiometer, or against simulated brightness temperatures from a radiative transfer model if the exact channel specifications are known, assuming radiative transfer model and surface emissivity model are free of systematic errors. However, also simulated brightness temperatures will have an uncertainty and both, observations and simulations can only agree within their given total uncertainties.

The total radiometer calibration error budget is composed of the following contributors: (a) warm target reference error, (b) cosmic background reference error, (c) radiometer/calibration nonlinearity, (d) errors in the APC coefficients (spill-over and polarization leakages), and (e) along-scan cross polarization mixing. An analysis of these error terms has been done by



	<b>Algorithm Theoretical Basis Document</b> <b>Microwave Imager Radiance FCDR R4</b> <b>SMMR Brightness Temperatures</b>	Doc. No: SAF/CMDWD/ATBD/FCDR_SMMR Issue: 2.3 Date: 2022-03-31
---	--	---

Hollinger (1989) and Colton and Poe (1999) for the SSM/I and will also be used here with some modifications for SMMR:

*a) Hot load reference error*

No information on pre-launch measurements of the temperature sensors is available. Therefore an absolute uncertainty of 0.1 K is assumed for the SMMR (same value as for SSM/I).

*b) Cosmic background reference error*

The SMMR suffers from periodic sunlight intrusion events into the cold sky calibration horns. This usually occurs once during each orbit over the southern polar region. These regions are not used in the calibration. Instead the cold counts are linearly interpolated between the last valid values. Apart from these events, it is believed that the SMMR calibration horns provide a clear view of the cosmic background. To account for these short-term intrusions an uncertainty of 0.1 K is assumed.

*c) Radiometer/calibration nonlinearity*

Nonlinearities in the calibration measurements and in the radiometer receiver may be expected to appear in the calibration data. At measurement temperatures equal to the calibration reference targets, the calibration uncertainty is the accuracy of the reference, which does show small systematic uncertainties (see above). At intermediate temperatures, radiometer nonlinearity and calibration reference temperature errors contribute to the total uncertainty with the errors weighted according to the temperature difference between the input and the calibration references. To test the radiometer absolute calibration, thermal vacuum tests have been conducted for the SMMR instrument at the Jet Propulsion Laboratory (JPL) for temperature levels ranging from 77 K to 320 K (Gloersen, 1987). Within the observed radiometer switch temperature range of  $\pm 2$  K the differences between linear and quadratic calibration equations are within 0.1 K for all channels.

*d) Errors in the APC coefficients (spill-over and polarization leakage)*

During the ground instrument calibration also a radiometric characterization of the antenna properties is performed. The accuracy of the derived APC coefficients is a function of the number of antenna range measurements, the dynamic range of the measurements, as well as the repeatability, accuracy, and stability of the antenna range transmitter/receiver over the measurement period. The estimated absolute accuracy of the feedhorn spill-over is 0.3-0.5% and the relative cross-polarization accuracy is in the order of 5-10% for the SSM/I (Colton and Poe, 1999). Without more information available on the SMMR, these values from the SSM/I are also taken for the SMMR. The uncertainty in the spill-over translates to a scene dependent uncertainty in the order of about 1-1.5 K at a 300 K scene temperature. The uncertainty in the cross-polarization accuracy results in an uncertainty which depends on the scene TB polarization difference and is in the order of 0.15-0.3 K for a scene polarization difference  $T_{Bv} - T_{Bh} = 50$  K.

*e) Along-scan cross polarization mixing*

Apart from the internal polarization mixing due to leakages, the SMMR TBs are also affected by scan-angle depending polarization mixing. Njoku et al. (1998) report the rms-errors of the

fitted correction coefficients to be between 0.046 K and 0.157 K. The remaining along-scan biases range between 0.2 K to 0.5 K (see section 4.4.1).

The individual systematic error contributions are summarized in Table II-3. The standard uncertainties  $u$  of the error terms  $y$  are estimated assuming a uniform distribution for a minimum and a maximum expected range of variation  $\Delta a$  (as estimated above):

$$u(y) = \frac{\Delta a}{\sqrt{3}}. \quad \text{Equation II-24}$$

The combined expected standard uncertainty of the systematic error

$$u_c(T_B) = \sqrt{\sum_i u_i^2(y)} \quad \text{Equation II-25}$$

is in the order of 0.4-1 K, with a significant dependence on the scene temperature and scene polarization.

## 4.8 Practical Considerations

### 4.8.1 Validation


A conclusion from the error budget estimation (see section 4.7) is that a complete comprehensive validation of the SMMR brightness temperatures is not possible. The final aim of an evaluation process must be, to show that the measured SMMR brightness temperatures are in agreement with modelled brightness temperatures within the expected total uncertainties. However, as a major requisite, a Fundamental Climate Data Record must show an improved quality compared to the existing raw data records in order to be a useful dataset providing an added value to the user community.

The FCDR of SMMR brightness temperatures will be compared to the original raw data records and to simulated brightness temperatures using reanalysis profiles. However, the reanalysis has already been used as the transfer target to bridge the gap to the SSM/I F08 (see section 4.6.1) and to derive along-scan corrections for the 37 GHz channels. These comparisons will therefore not be completely independent.

### 4.8.2 Quality control

The level 1B SMMR data records do contain a status flag, which is also provided in the final FCDR. Some additional QC flags are set as follows:

- All FOV brightness temperatures are tested and a FOV channel QC flag is set when
  - the TB is out of bounds:
    - 130 K < 18v, 21v, 37v;
    - 80 K < 18h < 300 K;
    - 110 K < 37h < 300 K,
  - the TB difference between vertical and horizontal polarization is out of bounds:
    - TBv – TBh < -20 K.

	<b>Algorithm Theoretical Basis Document</b> <b>Microwave Imager Radiance FCDR R4</b> <b>SMMR Brightness Temperatures</b>	Doc. No: SAF/CMDWD/ATBD/FCDR_SMMR Issue: 2.3 Date: 2022-03-31
---	--	---

- If more than 10 FOVs are flagged then the whole scan line is regarded as bad quality and the overall calibration QC flag is set accordingly.
- During the special operations period from April 3 to June 23, 1986 (see section 3.2) the data quality is significantly reduced and the scanline quality flag is set accordingly.

All scan lines remain in the file, so every user has the freedom to apply their own quality tests or to use the supplied quality flags to filter non valid data.

#### 4.8.3 Outputs (FCDR Product Definition)

The CM SAF FCDR of SMMR brightness temperatures is compiled as daily collections of all available observations. When the SMMR is operating at alternate days, orbits at the end of the day are completed and the file ends with the last scan from this orbit.

Organizing the data records in files with fixed start times simplifies the usage in climatological applications. The data files are archived in NetCDF format following NetCDF Climate and Forecast (CF) Metadata Convention version 1.7 (<http://cf-pcmdi.llnl.gov/documents/cf-conventions/1.7/cf-conventions.html>).


All sensor specific data and metadata records available in the level 1B data records are provided as well as additional information like quality control flags and inter-sensor calibration offsets. A detailed description of the product files will be given in the Product User Manual.

## 5 Assumptions and Limitations

The inter-sensor calibration method used here to correct the SMMR brightness temperatures (see section 4.6.1) does not account for an absolute radiometric offset. The inter-calibration target is the SSM/I aboard DMSP F08, which is inter-calibrated to the SSM/I F11 and acts as a transfer standard. Therefore, any absolute offset in the F11 TBs will be transferred to the other radiometers. However, one reason to choose the F11 as the reference target was its good performance when validating against collocated in-situ wind speed measurements from buoy observations. This should at least minimize the remaining absolute error in the brightness temperature data record.

The inter-sensor calibration is determined over ocean because of a lower variability, smaller diurnal cycle and better behaved error characteristics in the modelled brightness temperatures. Scene dependence is accounted for, assuming no systematic instrument related errors at the warm calibration target. Therefore, the quality of the inter-calibration is expected to be better over ocean than over land and sea-ice. Also, it is assumed that the inter-sensor differences can be characterized as a linear problem and the derived correction coefficients can be used over land and ice as well.

The inter-sensor calibration does not account for radiometric differences due to frequency shifts, EIA variations, or overpass time differences. The brightness temperatures are corrected to be physically consistent with the SSM/I observations. During the level 1B processing various corrections were applied to the antenna temperatures. Although these corrections might not be optimal or even incorrect, it is not possible to revert the original uncorrected temperatures.

	<b>Algorithm Theoretical Basis Document</b> <b>Microwave Imager Radiance FCDR R4</b> <b>SMMR Brightness Temperatures</b>	Doc. No: SAF/CMDWD/ATBD/FCDR_SMMR Issue: 2.3 Date: 2022-03-31
---	--	---

A number of limitations arise from the SMMR calibration problems. Francis (1987) provided a thorough analysis of these instrument related deficiencies, which are summarized here as follows:

*a) Polarization Mixing*

Due to the scan geometry the polarization vector relative to the Earth surface rotates with increasing scan angle and horizontally and vertically polarized radiation is mixed. Also leakages in the radiometer switches lead to polarization mixing.

*b) Sunlight intrusions*

During certain portions of the orbit, sunlight intrusions into the cold sky calibration occur. A quality status flag indicates this condition.

*c) In-orbit variation of instrument temperatures*

A warming trend over the first three orbits after the instrument is switched on can be observed when it is in alternate day operation mode. A quality status flag indicates this condition.

*d) Attitude variations*

Anomalies in the spacecraft attitude control system are observed. Amongst others, abrupt changes occur when the attitude control is switched from the daytime to the night-time system. These anomalies translate to anomalies in the observed EIA and therefore lead to uncertainties in the brightness temperatures.

*e) Component degradation*

Some channels are affected by continuous drifts in the brightness temperatures that can only be explained by drifts in the radiometer components over the life time. This affects mainly the 21 GHz channels. Although a correction was applied in the Level 1B processing to remove this effect, a significant artificial drift might still be observed in the final FCDR. This might compromise the suitability of this data record for climate trend analysis applications if the affected SMMR channels are utilised.

*f) Sun glitter reflection*


During certain portions of the daytime orbit, the observed brightness temperatures at the lower frequencies (6.6 and 10 GHz) are contaminated by reflected solar radiation from the surface.

*g) Faraday rotation*

Faraday rotation by the ionosphere is adding an additional polarization mixing during daytime observations. This affects mainly the 6.6 GHz channels.

## 6 References

- Andersson, A., Fennig, K., Klepp, C., Bakan, S., Graßl, H., and Schulz, J. (2010): The Hamburg Ocean Atmosphere Parameters and Fluxes from Satellite Data – HOAPS-3, *Earth Syst. Sci. Data*, 2, 215-234, doi:10.5194/essd-2-215-2010.
- Andersson, A., C. Klepp, K. Fennig, S. Bakan, H. Graßl, and J. Schulz (2011): Evaluation of HOAPS-3 ocean surface freshwater flux components, *Journal of Applied Meteorology and Climatology*, 50, 379-398, doi:10.1175/2010JAMC2341.1.
- Colton, M. C. and Poe, G. A. (1999): Intersensor Calibration of DMSP SSM/I's: F-8 to F-14, 1987–1997, *IEEE Trans. Geosci. Remote Sens.*, 37, 418–439.
- Fennig, K.; Andersson, A.; Schröder, M. (2013): Fundamental Climate Data Record of SSM/I Brightness Temperatures. Satellite Application Facility on Climate Monitoring. DOI:10.5676/EUM\_SAF\_CM/FCDR\_SSMI/V001.
- Fennig, K.; Andersson, A.; Schröder, M. (2015): Fundamental Climate Data Record of SSM/I / SSMIS Brightness Temperatures. Satellite Application Facility on Climate Monitoring. DOI:10.5676/EUM\_SAF\_CM/FCDR\_MWI/V002.
- Fennig, K., Schröder, M., Andersson, A., and Hollmann, R.: A Fundamental Climate Data Record of SMMR, SSM/I, and SSMIS brightness temperatures, *Earth Syst. Sci. Data*, 12, 647–681, <https://doi.org/10.5194/essd-12-647-2020>, 2020.
- Francis, E. A. (1987): Calibration of the Nimbus-7 Scanning Multichannel Microwave Radiometer (SMMR) 1979-1984. Master's Thesis, College of Oceanography, Oregon State University, Corvallis Oregon.
- Fu, C. C.; Han, D., Kim, S. T., Gloersen, P. (1988): User's Guide for the Nimbus-7 Scanning Multichannel Microwave Radiometer (SMMR) CELL-ALL Tape. NASA Reference Publication 1210, National Aeronautics and Space Administration, Washington, DC.
- GLOBE Task Team (1999): The Global Land One-kilometer Base Elevation (GLOBE) Digital Elevation Model, Version 1.0., Tech. Rep., National Oceanic and Atmospheric Administration, National Geophysical Data Center, 325 Broadway, Boulder, Colorado 80303, USA, <http://www.ngdc.noaa.gov/mgg/topo/globe.html>.
- Gloersen, P.; Barath, F. T. (1977): A Scanning Multichannel Microwave Radiometer for Nimbus-G and SeaSat-A. *IEEE J. Oceanic Eng.*, OE-2, 271-178.
- Gloersen, P.; Cavalieri, D. J., Soule, H. V. (1980): An alternate Algorithm for Correction of the Scanning Multichannel Microwave Radiometer Polarization Radiances Using Nimbus-7 Observed Data. NASA Technical Memorandum 84976, Goddard Space Flight Center, Greenbelt, MD.
- Gloersen, P. (1987): In-Orbit Calibration Adjustment of the Nimbus-7 SMMR. NASA Technical Memorandum 100678, National Aeronautics and Space Administration, Washington, DC.

	<b>Algorithm Theoretical Basis Document</b> <b>Microwave Imager Radiance FCDR R4</b> <b>SMMR Brightness Temperatures</b>	Doc. No: SAF/CMDWD/ATBD/FCDR_SMMR Issue: 2.3 Date: 2022-03-31
---	--	---

Gloersen, P.; Campbell, W. J., Cavalieri, D. J., Comiso, J. C., Parkinson, C. L., Zwally H. J. (1992): Arctic and Antarctic Sea Ice, 1978-1987: Satellite Passive Microwave Observations and Analysis. NASA SP-51, Goddard Space Flight Center, Greenbelt, MD.

Hollinger, J. (1989): DMSP Special Sensor Microwave/Imager Calibration/Validation I, Naval Research Laboratory, Washington, DC 20375-5000.

Hoots, F. R., Roehrich, L. R. (1988): "Models for Propagation of NORAD Element Sets", December 1988

Madrid et al. (1978): the Nimbus 7 Users' Guide, NASA Technical Memorandum 79969, , Goddard Space Flight Center, Greenbelt, MD.

Meunier, L. F.; English, S., Janssen, P. (2014): Improved ocean emissivity modelling for assimilation of microwave imagers using foam coverage derived from a wave model, EUMETSAT NWP SAF

Njoku, E. G.; Rague B., Fleming K. (1998): The Nimbus-7 SMMR Pathfinder Brightness Temperature Data Set, JPL Publication 98-4.

Njoku, E. G. (2003): Nimbus-7 SMMR Pathfinder Brightness Temperatures, Version 1., Boulder, Colorado USA. NASA National Snow and Ice Data Center Distributed Active Archive Center. DOI:10.5067/7Y1XWXT07HH8.

Poli P, and Co-authors (2013): The data assimilation system and initial performance evaluation of the ECMWF pilot reanalysis of the 20th-century assimilating surface observations only (ERA-20C). ERA Report Series 14, September 2013, 59 pp., available from ECMWF, Shinfield Park, Reading. <http://old.ecmwf.int/publications/library/do/references/list/782009>.

Poli, P.; Peubey C., Fennig K., Schröder M., Roebelling R., Geer A. (2015): Pre-assimilation feedback on a Fundamental Climate Data Record of brightness temperatures from Special Sensor Microwave Imagers: A step towards MIPs4Obs?, ERA Report Series, 19.

Saunders R.; Hocking J., Rundle D., Rayer P., Matricardi M., Geer A., Lupu C., Brunel P., Vidot J. (2013): RTTOV-11 science and validation report. EUMETSAT NWP SAF, 62pp. available from [http://nwpsaf.eu/deliverables/rtr/rtr\\_rtov11.html](http://nwpsaf.eu/deliverables/rtr/rtr_rtov11.html).

Sapiano, M. R. P, Berg, W. K., McKague, D. S., Kummerow, C. D. (2013): Toward an Intercalibrated Fundamental Climate Data Record of the SSM/I Sensors, IEEE Trans. Geosci. Remote Sens., 51, 1492–1503, DOI: 10.1109/TGRS.2012.2206601.

Wentz, F. J. (1991): User's Manual for SSM/I Antenna Temperature Tapes Revision 1, Technical Report 120191, Remote Sensing Systems, Santa Rosa, California.

## 7 Appendix A

**Table II-1:** Nimbus-7 SMMR characteristics (Nimbus-7 Users Guide, Madrid et al. 1978).

Channel	1,2	3,4	5,6	7,8	9,10
Frequency [GHz]	6.6	10.69	18.00	21.00	37.00
Bandwidth [Mhz]	250	250	250	250	250
Integration time [ms]	126	126	62	62	30
3-dB beamwidth [deg]	4.2	2.6	1.6	1.4	0.8
FOV resolution [km]	148x95	91x59	55x41	46x30	27x18
Sensitivity [K]	0.9	0.9	1.2	1.5	1.5
Absolute accuracy [K]	<2	<2	<2	<2	<2

**Table II-2:** Antenna spill-over fractions  $\delta$  and polarization mixing coefficients  $Q_v, Q_h, \gamma_v, \gamma_h$  (from Njoku et al., 1998).

Frequency [GHz]	6.6	10.7	18.0	21.0	37.0
$\delta_h$	0.04965	0.03477	0.02160	0.02284	0.01081
$\delta_v$	0.06553	0.04019	0.02259	0.02325	0.01330
$Q_h$	0.722	0.805	0.752	0.900	0.804
$Q_v$	0.791	0.842	0.763	0.869	0.705
$\gamma_h$	-4.81	-1.35	2.41	2.80	-0.26
$\gamma_v$	3.12	-0.43	-1.42	-10.93	-0.22

**Table II-3:** Summary of estimated systematic error source contributions.

Systematic error source	Systematic error [K]	Standard uncertainty [K]
Hot load reference	-	0.10
Cosmic background reference	-	0.10
Calibration non-linearity	—	0.10
Cross polarization (APC coefficients)	0.15 – 0.30	0.10 – 0.20
Feedhorn spill-over (APC coefficients)	1.00 – 1.50	0.60 – 0.90
Polarization mixing	0.20 – 0.50	0.10 – 0.30




## 8 Glossary

APC	Antenna Pattern Correction
ATBD	Algorithm Theoretical Baseline Document
CM SAF	Satellite Application Facility on Climate Monitoring
DMSP	Defense Meteorological Satellite Program
DWD	Deutscher Wetterdienst (German MetService)
ECI	Earth-centred inertial
ECMWF	European Centre for Medium Range Forecast
ECV	Essential Climate Variable
EIA	Earth Incidence Angle
EPS	European Polar System
EUMETSAT	European Organisation for the Exploitation of Meteorological Satellites
FCDR	Fundamental Climate Data Record
FMI	Finnish Meteorological Institute
FOV	Field of view
GCOS	Global Climate Observing System
GLOBE	The Global Land One-kilometer Base Elevation
HOAPS	The Hamburg Ocean Atmosphere Fluxes and Parameters from Satellite data
IOP	Initial Operations Phase
KNMI	Koninklijk Nederlands Meteorologisch Instituut
MD5	Message-Digest Algorithm 5
MSG	Meteosat Second Generation
NASA	National Aeronautics and Space Administration
NCEP	National Centers for Environmental Prediction
NDBC	National Data Buoy Center
NESDIS	National Environmental Satellite, Data, and Information System
NMHS	National Meteorological and Hydrological Services
NOAA	National Oceanic & Atmospheric Administration



NWP	Numerical Weather Prediction
PRD	Product Requirement Document
PUM	Product User Manual
QC	Quality Control
RMIB	Royal Meteorological Institute of Belgium
RMS	Root Mean Square
RSS	Remote Sensing Systems
SAF	Satellite Application Facility
SI	Système international d'unités
SMHI	Swedish Meteorological and Hydrological Institute
SMMR	Scanning Multichannel Microwave Radiometer
SSM/I	Special Sensor Microwave Imager
SSMIS	Special Sensor Microwave Imager Sounder
TA	Antenna Temperature
TB	Brightness Temperature
TDR	Temperature Data Records

	<b>Algorithm Theoretical Basis Document</b> <b>Microwave Imager Radiance FCDR R4</b> <b>SMMR Brightness Temperatures</b>	Doc. No: SAF/CMDWD/ATBD/FCDR_SMMR Issue: 2.3 Date: 2022-03-31
---	--	---

### III SSM/I

The algorithms and methods to build the SSM/I FCDR component have not been changed compared to the last release and are described in the corresponding ATBD [RD 1].

### IV SSMIS

The algorithms and methods to build the SSMIS FCDR component are described in the corresponding ATBD [RD 2]. The fourth release will include four additional years (2016-2019) of SSMIS observations from F16, F17, and F18.